Thermal Turbulence in Mercury

Tohru Takeshita, Takehiko Segawa, James A. Glazier,* and Masaki Sano
Research Institute of Electrical Communication, Tohoku University, Sendai 980, Japan
(Received 22 August 1995)

We studied thermal turbulence in a low Prandtl number, Pr, fluid using liquid Hg (Pr = 0.024). For Rayleigh numbers ($10^6 < \mathrm{Ra} < 10^8$), the histogram of temperature fluctuations at the center of the cell (aspect ratio 1), and the scaling laws for the Nusselt number and the large scale flow, all showed He-like hard turbulence. However, the cascade range of the frequency spectrum of the temperature fluctuations was smaller than expected. Direct measurement showed that the thermal and viscous boundary layers had crossed, which may explain the peculiar scaling.

PACS numbers: 47.20.–k, 47.27.Jv

Experimental studies on turbulence in thermal convection have [1–5] revealed a distinctive turbulent state called hard turbulence, characterized by the following: (1) The histogram of the temperature fluctuations at the center of the fluid has an exponential distribution. (2) Large scale bulk circulation coexists with turbulence. (3) The Nusselt number, Nu, the root mean square temperature fluctuation, and the mean velocity of the large scale flow all have power law dependence on the Rayleigh number, Ra, with scaling exponents different from classical theory [6]. (4) The temperature power spectrum decays as a power law with a slope close to -1.4 for $\mathrm{Ra} < 10^{11}$ and two slopes for $\mathrm{Ra} > 10^{11}$.

Theories explaining the scaling phenomena of hard turbulence assume distinct boundary layers for the temperature and the velocity (viscous sublayer) fields, and that the entire temperature drop occurs within the viscous sublayer [2,6,7]. The thickness of the thermal boundary layer, λ_T, should scale as $\lambda_T \sim 1/\mathrm{Nu} \sim \mathrm{Ra}^{-\gamma}$, provided that the thermal boundary layer is purely diffusive ($\gamma = 0.285 \pm 0.004$ in experiment and $2/7$ in the theory) [2,7]. On the other hand, the thickness of the viscous boundary layer, λ_v, can be estimated by dimensional analysis as $\lambda_v \sim 1/\mathrm{Re} \sim \mathrm{Ra}^{-\epsilon}$, with $\epsilon = 0.485 \pm 0.005$ in experiment [3]. These exponents imply that at high Rayleigh numbers the viscous boundary layer may become thinner than the thermal boundary layer, violating the hypothesis that the thermal boundary layer is diffusion limited. Shraiman and Siggia [7] conjectured that hard turbulence is unstable if crossing occurs. Therefore hard turbulence may not be asymptotic for high Ra, but an intermediate. The relation $\mathrm{Nu} \sim \mathrm{Ra}^{1/2}$ was predicted for the new state [6–8]. Recent direct measurements of boundary layers in pressurized SF_6 confirmed the dependence of λ_T and λ_v on Ra, and showed that the crossing should take place around $\mathrm{Ra} \sim 10^{14}$, though these Ra were not obtained [9]. However, the Prandtl numbers of Belmonte, Tilgner, and Libchaber's [9] fluids were fairly high: Pr = 0.7 for helium and compressed gas, $2 < \mathrm{Pr} < 7$ for water. The lower the Prandtl number, the smaller the ratio of the boundary layer thicknesses, λ_v/λ_T, since the Reynolds number is higher. The critical Rayleigh number for this turbulence transition for liquid Hg (Pr = 0.024) should be $\mathrm{Ra} \sim 10^5$–10^7 [7]. In this Letter we examine the statistical and scaling properties of low Prandtl number fluid (Hg) turbulence. We compare our results to hard turbulence in helium and pressurized gas. The Reynolds number of the flow is about 10 times higher than for He at the same Ra. Scaling behaviors are the same as for hard turbulence, except for the peculiar power spectrum scaling, which results from the viscous boundary layer being as thin or thinner than the thermal boundary layer.

The experimental cell is a vertical cylinder 10 cm in height and 10 cm in diameter (aspect ratio 1). The top and bottom plates are made of nickel plated copper 2 cm thick. The side wall cylinder is made of stainless steel 2 mm thick to match the thermal conductivity of Hg. The high thermal conductivity of mercury requires special heating and cooling. In the bottom plate, an insulated manganin wire heater (diameter 0.3 mm) is embedded with thermal conducting paste in a spiral groove of semicircular section, width 0.4 mm and spacing 0.6 mm. The top plate forms the bottom of a large copper container with many copper fins embedded to promote good thermal exchange with the cooling water. Temperature controlled water enters the container through five inlets and exits from four outlets. The heater is supplied with constant power ranging from 1 W to several hundred watts depending on the target Rayleigh number. The temperature of the cooling water is controlled in stages: first by a refrigerator and an electric heater, second by a 20 liter ballast tank, and finally by Peltier elements for precise control. The worst temperature stability occurs for maximal heating and is 1% of the total temperature difference, ΔT, between the top and bottom plates. The best stability occurs for minimal heating and is of the order of 10^{-4} K. To measure the local temperature fluctuations, we used four thermistors with diameter 400 μm and length 1 mm. Their response time is less than 50 msec, sufficiently shorter than the flow's typical minimum time scale of 100–200 msec. As shown in Fig. 1, one (A) is placed at the center of the cell at midheight, two are vertically aligned at 1 cm from

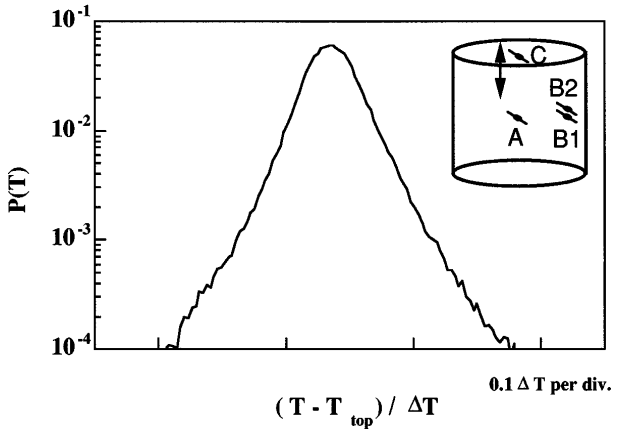

FIG. 1. Nearly exponential histogram of temperature fluctuations measured by the center thermistor (A) at Ra $= 7.54 \times 10^7$. The inset shows a schematic drawing of the experimental cell with the positions of the thermistors.

the side wall, one at midheight ($B1$), and the other 2 mm above ($B2$) to measure the mean flow velocity. The fourth detector (C) may be moved vertically along the center line of the cylinder to determine the boundary layer profile. Each thermistor constitutes one arm of an ac capacitance bridge whose output is fed to a lock-in amplifier (PAR 124A). The output signal is first digitized and stored in an HP digital spectrum analyzer (HP3563A) then analyzed by computer.

The histogram of the temperature fluctuations is close to an exponential distribution for accessible Rayleigh numbers, $10^6 <$ Ra $< 10^8$, verifying that the turbulence is well developed. Figure 1 shows the histogram of the temperature fluctuations at the center of the cell (A) for Ra $= 7.54 \times 10^7$. Large scale circulation persists over the same range of Rayleigh numbers. We measured the mean flow velocity of the large scale circulation with two adjacent thermistors ($B1$, $B2$) near the side wall. We estimated the group velocity of temperature fluctuations passing through the two detectors from the phase delay of the cross spectrum of the two signals [3]. The mean flow velocity was about 2 cm/sec at Ra $= 10^7$. We obtained the Reynolds number at length L from the mean flow velocity V; Re $= VL/\nu$ in Fig. 2. The large scale circulation rather than any secondary instability (e.g., the oscillatory instability) causes the frequency peak of the temperature power spectrum, f_p [3]. Thus f_p also gives an estimate of the mean flow velocity, using the relation $V \sim \pi L f_p$. We also plot the dimensionless parameter $\mathrm{Re}' \equiv f_p \pi L^2/\nu$ in Fig. 2. Direct and indirect measurements of mean flow velocity coincide. The scaling relation $V/(\nu/L) \sim 6.24\mathrm{Ra}^{0.47\pm0.02}$ resembles hard turbulence in He but with a coefficient 20 times larger.

Reference [3] estimates that the transition to hard turbulence takes place when the Reynolds number of the box exceeds 10^3. As shown in Fig. 2, Re is 10^4 at Ra $\sim 10^7$. Thus, even the lowest Ra (10^6) in our experiment is well

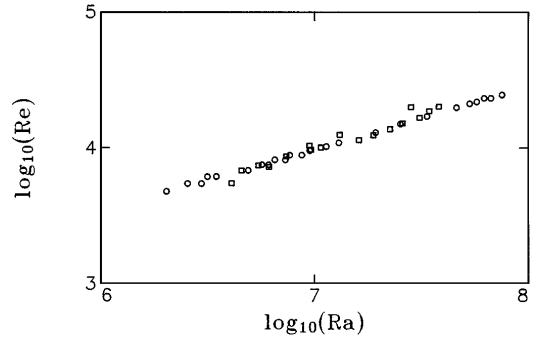

FIG. 2. Scaling of the Reynolds number of the box, Re $= VL/\nu$, as a function of the Rayleigh number (rectangles). The mean flow velocity can be estimated from the frequency peak, f_p. The Reynolds number is compared to $\pi f_p L^2/\nu$ (circles). Both quantities fit the scaling $\mathrm{Re} = 6.24\mathrm{Ra}^{0.46\pm0.02}$.

within the hard turbulence regime. Extrapolating to a lower Rayleigh number suggests that hard turbulence in mercury starts around Ra $\sim 10^5$, not far from the onset of convection and chaos. Soft turbulence may occur over a narrow range or not exist in low Pr number fluids.

Figure 3 shows the power spectrum of temperature fluctuations at Ra $= 7.12 \times 10^7$. We fit the power spectrum with a function [4],

$$P(f) = \left(\frac{f}{f_0}\right)^{-\alpha} \exp\left(-\frac{f}{f_c}\right). \tag{1}$$

By fitting power spectra for Ra numbers ($10^7 <$ Ra $< 10^8$), we obtain $\alpha = 1.58 \pm 0.09$. We plot the cutoff frequency, f_c, as a function of Ra in Fig. 4. f_c scales as $f_c \sim \mathrm{Ra}^{\beta}$, with $\beta = 0.4 \pm 0.05$. The exponent differs from that of He turbulence where $\beta = 0.78$ by the same method [10]. We can understand the exponent β in the He experiment as follows: the cutoff frequency depends on the smallest spatial structure (plume) of size Λ advected by the mean flow velocity, V. Thus $f_c \sim V/\Lambda$. Λ should be of the same order as the thickness of the thermal boundary layer, λ_T. Therefore $f_c \sim \mathrm{Ra}^{\gamma+\epsilon} \Rightarrow \beta = \gamma + \epsilon$ for

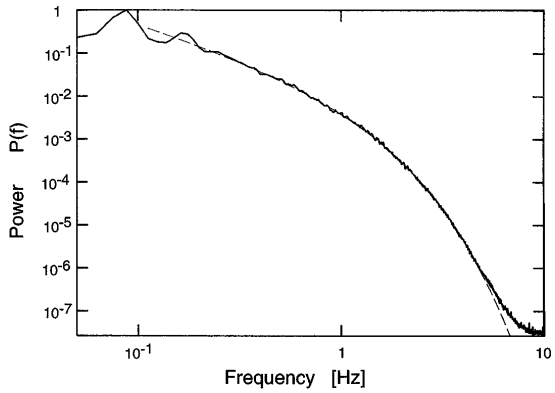

FIG. 3. Frequency power spectrum of the side thermistor ($B1$) at Ra $= 7.12 \times 10^7$. The dotted line shows a fit by the function $P(f) = P_0(f/f_0)^{-\alpha} \exp[-(f/f_c)]$, $\alpha = 1.49$.

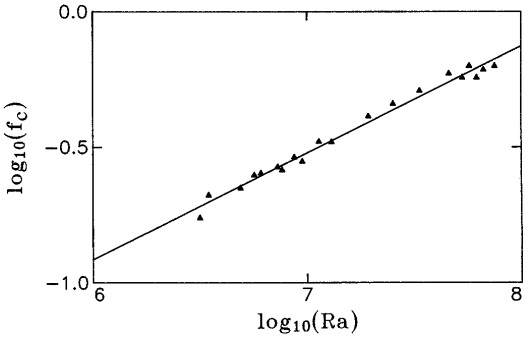

FIG. 4. Scaling of the cutoff frequency, f_c, as a function of Ra. The dotted line is the best fit, $f_c \sim \mathrm{Ra}^{0.40\pm0.06}$.

He and SF_6 turbulence. However, the argument fails for mercury turbulence.

As shown in Fig. 2, the frequency peak f_p scales as $f_p \sim \mathrm{Ra}^{0.46\pm0.02}$. Comparing the scaling exponents for f_p and f_c in Hg shows that the entropy cascade range [11–13] of the power spectrum unexpectedly shrinks with increasing Ra. This difference in scaling is the main puzzle of Hg turbulence.

We calculated the Nusselt number, Nu, from the power supplied to the bottom plate heater. The convection cell is surrounded by a thermal insulator and placed in a stainless steel outer jacket whose bottom temperature is set to the temperature of the bottom plate heater of the cell to minimize heat leakage. Correcting the heat leak along the side wall gives the heat flux through the mercury. Figure 5 shows the Nusselt number as a function of the Rayleigh number. The solid line shows the $2/7$ scaling relation. The best fit to the data gives $\mathrm{Nu} = 0.155\mathrm{Ra}^{0.27\pm0.02}$. As found by other researchers [14,15], the coefficient is smaller than for He which is inconsistent with the prediction of Shraiman and Siggia [7].

We measured the thermal boundary layer and the viscous boundary layer directly, using a thermistor suspended by a thin frame and moved vertically along the center line of the cylindrical cell by a stepper motor. We plot the time average of the temperature, T, as a function of the distance from the top plate z in Fig. 6(a). Temperature profiles fit the function $T_{\mathrm{ave}}(z) - T_{\mathrm{top}} = m_1 \tanh(m_2 z)$, which satisfies the requirement of linearity near to and saturation far from the boundary. We define the thermal boundary layer thickness as $\lambda_T = 1/m_2$ from the fit. Thus λ_T is the distance at which the extrapolation of the linear part of the profile equals the central mean temperature. The estimated thickness also agrees with the distance at which the root mean square of the temperature fluctuations, T_{rms}, reaches its maximum, as shown in Fig. 6(a). We find $\lambda_T = 4.0$ mm at $\mathrm{Ra} = 3.5 \times 10^7$.

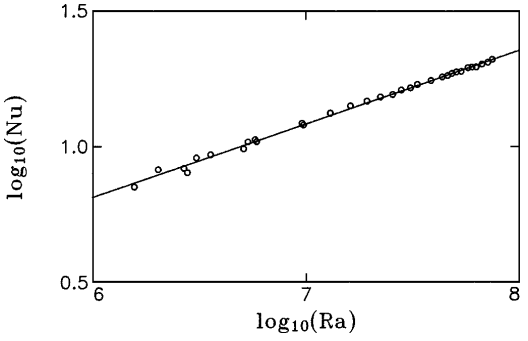

FIG. 5. Scaling of the Nusselt number as a function of Ra. The solid line is the slope $(2/7)$.

We estimated the profile of the viscous boundary layer from the highest frequency, f_h, of the temperature frequency spectrum. Measurements in water and SF_6 [9,16] have validated this method. In Fig. 6(b), we show f_h as a function of the distance z. As the viscous boundary layer thickness we took the distance at which f_h is maximal to obtain $\lambda_v = 2.7$ mm at $\mathrm{Ra} = 3.5 \times 10^7$, so $\lambda_v \sim 0.7\lambda_T$. This ratio differs in pressurized SF_6 for which λ_v is much larger than λ_T (for instance $\lambda_v \sim 3\lambda_T$). Evidently the two boundary layers have crossed at this Ra. Further

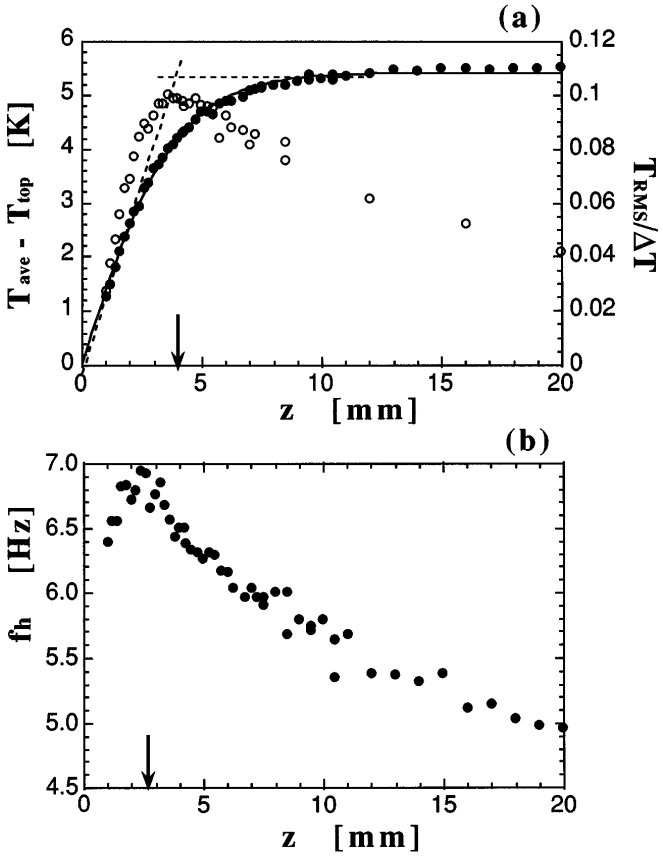

FIG. 6. (a) Temperature profile (dots) and root mean square fluctuation (circles) near the top plate, measured by the movable thermistor (C). The solid line is the best fit by a function, $T_{\mathrm{ave}}(z) - T_{\mathrm{top}} = m_1 \tanh(m_2 z)$. The guide line shows the thermal boundary layer thickness. (b) The profile of the frequency, f_h, as a function of the distance, z, from the top plate. The distance at which f_h reaches its maximum approximates the viscous boundary layer thickness.

experimental study of the Ra dependence of the boundary layers is in progress.

We can estimate the Reynolds number of the shear flow based on boundary layer thickness to be $\mathrm{Re}_\lambda \sim 500$, using $\lambda_v \sim 3$ mm, so the boundary layer is turbulent. Considering that the turbulent viscous boundary layer is as thin as or thinner than the thermal boundary layer, the plumes are stretched and mixed by the turbulent shear as soon as they detach from the thermal boundary layer and before they arrive at the center of the fluid. Therefore simple plumes may not exist in low Prandtl number fluids.

The diffusion time for a plume of size τ_T is $\tau_T = \lambda_T^2/\kappa$, where κ is the thermal diffusivity of the fluid. The advection time is $\tau = L/V$. Therefore the ratio of the two time scales characterizes the importance of diffusion:

$$\frac{\tau_T}{\tau} = \frac{\lambda_T}{L}\frac{U\lambda_T}{\kappa} = \frac{\lambda_T}{L}\,\mathrm{Pe}\,, \tag{2}$$

where Pe is the Peclet number for the thermal boundary layer. Using the estimates $\kappa = 4.3 \times 10^{-2}$ cm^2/sec, $\lambda_T \sim 5$ mm, and $V \sim 2$ cm/sec, we obtain $\tau_T/\tau \sim 0.5$, so we must consider effects of thermal diffusion. Turbulence may further increase the effective thermal diffusion.

Additionally, the surface (boundaries and side walls) and bulk flows lie in different regimes. The typical temperature fluctuation (rms) at the center, θ, is about 3% of the total temperature difference, ΔT; thus $\theta/\Delta T \sim 10^{-2}$ at $\mathrm{Ra} = 10^7$. The typical velocity is about 2 cm/sec at $\mathrm{Ra} \sim 10^7$. The buoyancy force, $\alpha g\theta$, of the fluctuation at the center is much smaller than the inertial term, $|U\nabla U| \sim U^2/L$; $\alpha g\theta/(U^2/L) \sim 10^{-2}$, where α is the thermal expansion coefficient and g is the gravitational acceleration. Therefore, in the center region, buoyancy is negligible and temperature fluctuations resemble a passive scalar, perhaps causing the scaling behavior of the spectrum. We obtain a correct estimate (2 cm/sec) of the mean flow velocity by balancing the buoyancy of the boundary layer, $\alpha g\Delta T$, with the inertial term, U^2/L; implying that most of the detached boundary layer flows along the side wall in the large scale circulation, which drives the turbulent flow in the center. At larger scales inertia balances the buoyancy term, while at smaller scales inertia balances the energy transfer. The Bolgiano scale, L_B, at which buoyancy and energy transfer are of the same order, is given by $L_B = \mathrm{Nu}^{1/2}L/(\mathrm{Ra}\,\mathrm{Pr})^{1/4}$ [17]. In the experiment $L_B \sim 2$ cm at $\mathrm{Ra} = 10^7$ which corresponds to 1 Hz in the spectrum, narrowing the cascade range.

We did not observe a transition to $\mathrm{Nu} \sim \mathrm{Ra}^{1/2}$.

We are grateful to M. Sugawara for building the experimental cell and to Y. Sawada, P. Tabeling, and A. Naert for stimulating discussions. This work was supported by Japanese Grant-in-Aid for Science Research Fund from the Ministry of Education, Science and Culture (No. 07832002 and No. 05232102). J. A. G. acknowledges support and hospitality from Tohoku University and the support of NSF Grants No. DMR92-57011 and No. INT91-01345 and the ACS/PRF.

*Permanent address: Department of Physics, University of Notre Dame, Notre Dame, IN 46556-5670.

[1] F. Heslot, B. Castaing, and A. Libchaber, Phys. Rev. A **36**, 5870 (1987).
[2] B. Castaing *et al.*, J. Fluid Mech. **204**, 1 (1989).
[3] M. Sano, X. Z. Wu, and A. Libchaber, Phys. Rev. A **40**, 6421 (1989).
[4] X. Z. Wu, L. P. Kadanoff, A. Libchaber, and M. Sano, Phys. Rev. Lett. **64**, 2140 (1990).
[5] T. H. Solomon and J. P. Gollub, Phys. Rev. Lett. **64**, 2382 (1990); Phys. Rev. A **43**, 6683 (1991).
[6] W. V. R. Malkus, Proc. R. Soc. London A **225**, 185 (1954); L. N. Howard, J. Fluid Mech. **17**, 405 (1963).
[7] B. I. Shraiman and E. D. Siggia, Phys. Rev. A **42**, 3650 (1990).
[8] R. Kraichnam, Phys. Fluids **5**, 1374 (1962).
[9] A. Belmonte, A. Tilgner, and A. Libchaber, Phys. Rev. Lett. **70**, 4067 (1993); Phys. Rev. E **50**, 269 (1994).
[10] X. Z. Wu, Ph.D. thesis, The University of Chicago, 1991.
[11] R. Bolgiano, Jr., J. Geophys. Res. **64**, 2226 (1962); **64**, 3023 (1962).
[12] A. M. Obukhov, Dokl. Akad. Nauk. SSSR **121**, 1246 (1959) [Sov. Phys. Dokl. **3**, 61 (1959)].
[13] A. Brandenburg, Phys. Rev. Lett. **69**, 605 (1992); V. Yakhot, Phys. Rev. Lett. **69**, 769 (1992); S. Toh and E. Suzuki, Phys. Rev. Lett. **73**, 1501 (1994).
[14] S. Globe and D. Dropkin, J. Heat Transfer **31**, 24 (1959).
[15] S. Cioni, S. Ciliberto, and J. Sommeria, Dynamics of Atomospheres and Oceans (to be published).
[16] A. Tilgner, A. Belmonte, and A. Libchaber, Phys. Rev. E **47**, 2253 (1993).
[17] R. Benzi, R. Tripiccione, F. Massaioli, S. Succi, and S. Ciliberto, Europhys. Lett. **25**, 341 (1994). Since submitting this paper we have learned of similar results for the Bolgiano scale [S. Cioni, S. Ciliberto, and J. Sommeria, Europhys. Lett. (to be published)].